JOURNAL OF GUIDANCE, CONTROL, AND DYNAMICS
Vol. 24, No. 5, September–October 2001

Analysis of Piezoelectric Sensor to Detect Flexural Waves

M. Veidt,* T. Liu,† and S. Kitipornchai‡
University of Queensland, Brisbane, Queensland 4072, Australia

The electromechanical transfer characteristics of adhesively bonded piezoelectric sensors are investigated. By the use of dynamic piezoelectricity theory, Mindlin plate theory for flexural wave propagation, and a multiple integral transform method, the frequency-response functions of piezoelectric sensors with and without backing materials are developed and the pressure-voltage transduction functions of the sensors calculated. The corresponding simulation results show that the sensitivity of the sensors is not only dependent on the sensors' inherent features, such as piezoelectric properties and geometry, but also on local characteristics of the tested structures and the admittance and impedance of the attached electrical circuit. It is also demonstrated that the simplified rigid mass sensor model can be used to analyze successfully the sensitivity of the sensor at low frequencies, but that the dynamic piezoelectric continuum model has to be used for higher frequencies, especially around the resonance frequency of the coupled sensor–structure vibration system.

Introduction

In the last decade an effective new approach for active control of structural vibrations has been developed and successfully applied to beam, plate, and other types of structures by, for example, Fuller et al.,[1] Miller and Hall,[2] Pan and Hansen,[3] and Fujii et al.[4] It is based on the interpretation of the dynamic response of the structures in terms of traveling stress waves rather than the traditional vibration modal summation method. In this study, the wave sensing problem involved in these techniques is considered with the aim of quantifying the electromechanical transduction characteristics and, hence, to improve the efficiency of the traveling wave control techniques.

Although traveling wave concepts have been used in the design of control architectures before,[5] the wave sensing characteristics have not been studied in great detail, especially at higher frequencies and for composite structures. The common practice of employing standard accelerometers as output devices is, in fact, insufficient because, due to wave scattering effects, the output voltage of the sensor is not only dependent on the characteristics of the sensor alone but also on the dynamic behavior of the structure. Therefore, to enable the inclusion of high-frequency components that arrive earlier and, thus, are essential to enable the design of optimized control systems, the sensors need to be particularly designed according to the characteristics of the structure to be controlled. In this paper, the sensing characteristics of piezoelectric sensors to flexural waves in elastic plates are investigated. By the use of the dynamic theory of piezoelectricity, Mindlin plate wave motion theory, and a multiple integral transform method, the influence of the sensors' inherent features, such as piezoelectric properties and geometry, the tested structures and the attached electric circuit are examined.

Formulation of the Problem

As shown in Fig. 1, a piezoelectric crystal disk with top and bottom surface electrodes is attached to an isotropic plate. It is used to detect incoming flexural waves generated by an arbitrary external disturbance. As illustrated in Fig. 2, the z_1-coordinate axis is parallel to the poling axis of the longitudinal transducer and directed normal to the upper, traction-free, and lower, adhesively bonded, circular surfaces. The two electrodes are connected to an electronic measurement circuit of admittance Y.

In the following section, the input–output transfer characteristics between the incoming flexural wave and the output voltage of the piezoelectric sensor are determined. In this investigation a dynamic one-dimensional piezoelectric model is used to approximate the electromechanical transduction characteristics of the piezoelectric sensor. This means that except for the extensional stress and the electric displacement along the thickness, all stress and electric displacement components in the piezoelectric disk vanish, either exactly or approximately. Thus, according to the linear theory of piezoelectricity[6,7] the following equations hold, including the stress equation of motion,

$$\frac{\partial T_{zz1}}{\partial z_1} = \rho_1 \frac{\partial^2 w_1}{\partial t^2} \tag{1}$$

the charge equation of electrostatics,

$$\frac{\partial D_{z1}}{\partial z_1} = 0 \tag{2}$$

the strain displacement relation,

$$S_{zz1} = \frac{\partial w_1}{\partial z_1} \tag{3}$$

the quasi-static potential,

$$E_{z1} = -\frac{\partial \phi}{\partial z_1} \tag{4}$$

and the piezoelectric constitutive relations

$$S_{zz1} = s_{33}^E T_{zz1} + d_{33} E_{z1} \tag{5a}$$

$$D_{z1} = d_{33} T_{zz1} + \varepsilon_{33}^T E_{z1} \tag{5b}$$

where t denotes time; $w_1(z_1)$, $S_{zz1}(z_1)$, and $T_{zz1}(z_1)$ are the mechanical displacement, strain, and stress in the piezoelectric transducer, respectively; D_{z1}, E_{z1}, and ϕ represent the electric displacement and electric potential in the z_1 direction and a scalar electric potential, respectively; and ρ_1, S_{33}^E, d_{33}, and ε_{33}^T are the mass density, the elastic compliance, piezoelectric charge constant, and dielectric constant of the piezoelectric sensor, respectively.

In previous investigations of the wave control techniques[1] the classical thin plate theory has been used to model the behavior of the flexural waves. To analyze accurately the wave sensing characteristics of the piezoelectric crystal sensor, the Mindlin plate theory is employed in this study. Thus, in the Cartesian coordinate system (x, y, z) with the x and y axes lying in the plane of the plate and its origin in the midplane of the plate as shown in Fig. 3, the propagation behavior of the flexural waves is described by, for example,[8]

Received 23 March 2000; revision received 3 February 2001; accepted for publication 7 April 2001.

*Senior Lecturer, Department of Mechanical Engineering; veidt@mech.uq.edu.au.
†Research Associate, Department of Civil Engineering.
‡Professor, Department of Civil Engineering.

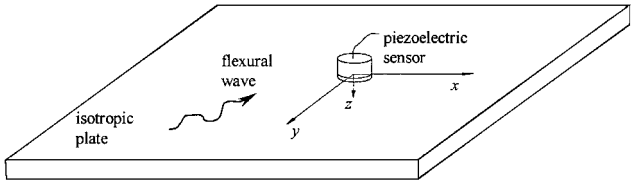

Fig. 1 Piezoelectric sensor adhesively attached to plate for flexural wave detection.

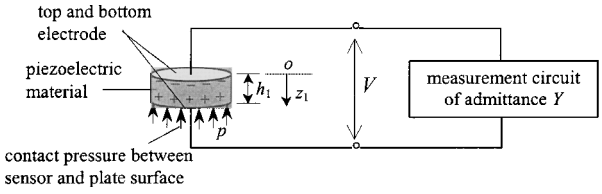

Fig. 2 Details of piezoelectric sensor, some of the major electrical and mechanical model parameters, and local sensor coordinate system introduced.

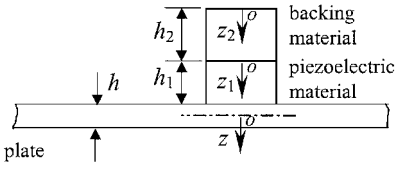

Fig. 3 Schematic of piezoelectric sensor with backing material attached to plate; coordinate systems used.

$$\left(\nabla^2 - \frac{\rho}{G'}\frac{\partial^2}{\partial t^2}\right)\left(D\nabla^2 - \frac{\rho h^3}{12}\frac{\partial^2}{\partial t^2}\right)w(x, y, t) + \rho h\frac{\partial^2 w(x, y, t)}{\partial t^2}$$

$$= \left(1 - \frac{D}{G'h}\nabla^2 + \frac{\rho h^2}{12G'}\frac{\partial^2}{\partial t^2}\right)q(x, y, t) \tag{6}$$

in which

$$\nabla^2 = \frac{\partial^2}{\partial x^2} + \frac{\partial^2}{\partial y^2} \tag{7a}$$

$$G' = k^2 G \tag{7b}$$

$$D = \frac{Eh^3}{12(1-\nu^2)} \tag{7c}$$

where t is the time variable; $w(x, y, t)$ the transverse deflection of the plate; k^2 is a correction factor relating to Rayleigh surface waves given by $0.76 + 0.3\nu$; E, G, and ν are Young's modulus, shear modulus, and Poisson's ratio; ρ is the material density; h is the plate thickness; and q the distributed forces exerted on the surface of the plate by external disturbances and the sensor.

Determination of Frequency-Response Functions of Bonded Sensor

In the traveling wave control technique, the vibration behavior of the structure whose dynamic response has to be optimized is characterized by the propagation behavior of stress waves. In the case of small deformations and linear elasticity, their motion can be readily analyzed as the superposition of harmonic plane waves of different frequencies and different wave numbers. In the following paragraphs, the sensing characteristics of contact-type piezoelectric transducers used as sensors in the control loop are derived. As indicated in Fig. 1, an arbitrary incident harmonic plane wave

$$w_{\text{in}}(x, y, t) = A_0 \exp[i(\kappa_x x + \kappa_y y - \omega t)] \tag{8}$$

is assumed to propagate toward the sensor, where A_0 is an arbitrary amplitude constant, ω is the circular frequency, and κ_x and κ_y are wave numbers in the directions of x and y, respectively. It is obvious that w_{in} satisfies Eq. (6), that is, the wave numbers κ_x and κ_y and the frequency ω must satisfy the dispersion equation of the plate, which can be easily obtained by substituting Eq. (8) into Eq. (6).

When the incident wave w_{in} arrives at the sensor, a scattered wave field w_s is generated by the sensor. The scattered wave field is introduced as

$$w_s(x, y, t) = \bar{w}_s(x, y, \omega)e^{-i\omega t} \tag{9}$$

where $\bar{w}_s(x, y, \omega)$ is an unknown function. Because of the electromechanical coupling, this mechanical disturbance will lead to an electrical output. In the following subsections, the electromechanical coupling characteristics of the sensor and the mechanical coupling between the sensor and the plate will be analyzed to determine the electrical voltage output of the sensor as a function of the incident wave.

Analysis of Sensor

The electromechanical coupling characteristics of the piezoelectric sensor are analyzed by the application of dynamic piezoelectricity theory. Substituting Eq. (3) into Eq. (5a) and then substituting the resultant equation into Eq. (1) yields

$$\frac{1}{s_{33}^E}\frac{\partial^2 w_1}{\partial z_1^2} - \frac{d_{33}}{s_{33}^E}\frac{\partial E_{z1}}{\partial z_1} = \rho_1\frac{\partial^2 w_1}{\partial t^2} \tag{10}$$

Similarly, substituting Eq. (3) into Eq. (5b) and then substituting the resultant expression into Eq. (2) yields

$$\frac{d_{33}}{s_{33}^E}\frac{\partial^2 w_1}{\partial z_1^2} + \left(\varepsilon_{33}^T - \frac{d_{33}^2}{s_{33}^E}\right)\frac{\partial E_{z1}}{\partial z_1} = 0 \tag{11}$$

Eliminating the term E_{z1} in Eqs. (10) and (11) results in the following equation of motion:

$$\bar{c}_{33}\frac{\partial^2 w_1}{\partial z_1^2} = \rho_1\frac{\partial^2 w_1}{\partial t^2} \tag{12}$$

in which

$$\bar{c}_{33} = \left(1/s_{33}^E\right)(1 + \chi^2) \tag{13a}$$

and

$$\chi^2 = d_{33}^2/\left(\varepsilon_{33}^T s_{33}^E - d_{33}^2\right) \tag{13b}$$

In addition, the following expressions for the other mechanical and electrical variables are derived:

1) By the integration of Eq. (1) with respect to z_1, the stress variable $T_{zz1}(z_1)$ can be expressed as

$$T_{zz1} = \int \rho\frac{\partial^2 w_1^2}{\partial z_1^2}\,\mathrm{d}z_1 \tag{14}$$

2) From Eqs. (3) and (5a), the electric field can be evaluated as

$$E_{z1} = \frac{1}{d_{33}}\frac{\partial w_1}{\partial z_1} - \frac{s_{33}^E}{d_{33}}T_{zz1} \tag{15}$$

3) When Eq. (5a) is substituted into Eq. (5b), and Eq. (3) is noted, the electric displacement can be expressed as

$$D_{z1} = \frac{d_{33}}{s_{33}^E}\frac{\partial w_1}{\partial z_1} + \left(\varepsilon_{33}^T - \frac{d_{33}^2}{s_{33}^E}\right)E_{z1} \tag{16}$$

The upper and lower electrode surfaces are considered to operate into a measurement circuit of admittance Y, as shown in Fig. 2. The electric current in the circuit can be obtained as

$$I = \frac{\mathrm{d}}{\mathrm{d}t}\int_A D_{z1}\,\mathrm{d}A = YV \tag{17}$$

where A represents the area of the upper or lower electrode surface and the voltage V is given by a potential difference as

$$V = \Delta\phi = \phi|_{z1=h_1} - \phi|_{z1=0} \tag{18}$$

When Eq. (4) is integrated with respect to z_1, the potential difference can be evaluated as

$$\Delta\phi = -\int_0^{h_1} E_{z1}\,\mathrm{d}z_1 \tag{19}$$

In view of Eqs. (14–19), it can be seen that by solving for the mechanical displacement $w_1(z_1)$ all of the other system variables and, specifically, the output voltage V will be obtained accordingly.

Applying the Fourier transform defined as

$$\bar{g}(\omega) = \int_0^{\infty} g(t)e^{-i\omega t}\,\mathrm{d}t \tag{20}$$

to Eq. (12) yields

$$\frac{\partial^2 \bar{w}_1}{\partial z_1^2} + c_1^2\omega^2\bar{w}_1 = 0 \tag{21}$$

where $c_1 = \sqrt{(\rho_1/\bar{c}_{33})}$.

From Eq. (21), the frequency-domain solution of the displacement $w_1(z_1)$ or, in other words, the wave motion within the piezoelectric disk, can be expressed as

$$\bar{w}_1 = A_1 e^{ic_1\omega z_1} + B_1 e^{-ic_1\omega z_1} \tag{22}$$

where $A_1(\omega)$ and $B_1(\omega)$ are currently still unknown. Note that because the wave motion within the piezoelectric disk is considered, the model can be used to analyze thick as well as thin sensors.

Applying the Fourier transform (20) to Eq. (14) and making use of Eq. (22) results in

$$\bar{T}_{zz1} = ic_1\bar{c}_{33}\omega\left(A_1 e^{ic_1\omega z_1} - B_1 e^{-ic_1\omega z_1}\right) + \gamma_1 \tag{23}$$

where $\gamma_1(\omega)$ is unknown.

Similarly, when the Fourier transform is applied to Eq. (15) and Eq. (23) is noted, the frequency-domain solution of the electric field can be expressed as

$$\bar{E}_{z1} = -\left(i\omega c_1\chi^2/d_{33}\right)\left(A_1 e^{ic_1\omega z_1} - B_1 e^{-ic_1\omega z_1}\right) - \left(s_{33}^E/d_{33}\right)\gamma_1 \tag{24}$$

The frequency-domain solution of the electric displacement is obtained by applying the Fourier transform to Eq. (16) and then substituting Eqs. (22) and (24) into the resultant equations,

$$\bar{D}_{z1} = \left(d_{33}/\chi^2\right)\gamma_1 \tag{25}$$

When the Fourier transform is applied to Eqs. (18) and (19) and Eq. (24) is used, the frequency-domain solution of the output voltage of the sensor can be expressed as

$$\bar{V} = \left(\chi^2/d_{33}\right)\left(e^{ic_1\omega h_1} - 1\right)A_1 + \left(\chi^2/d_{33}\right)\left(e^{-ic_1\omega h_1} - 1\right)B_1 + \left(s_{33}^E h_1/d_{33}\right)\gamma_1 \tag{26}$$

In addition, the frequency-domain solution of the output voltage of the sensor can be derived by applying the Fourier transform to Eq. (17) and using Eq. (25)

$$\bar{V} = \frac{id_{33}A\omega}{\chi^2 Y}\gamma_1 \tag{27}$$

When Eqs. (26) and (27) are compared, the $\gamma_1(\omega)$ can be expressed as

$$\gamma_1 = \mu_1\left[(e^{ic_1\omega h_1} - 1)A_1 + (e^{-ic_1\omega h_1} - 1)B_1\right] \tag{28}$$

in which $\mu_1(\omega)$ is given by

$$\mu_1 = \frac{\chi^2}{i\left(d_{33}^2 A\omega/\chi^2 Y\right) - s_{33}^E h_1} \tag{29}$$

Thus, the frequency-domain solutions of all mechanical and electrical variables can be expressed as functions of the two unknowns $A_1(\omega)$ and $B_1(\omega)$. To obtain these two unknowns, the behavior of the incident and scattered stress waves at the sensor location needs to be considered.

Mechanical Consideration of Plate

To evaluate the scattered wave field in the plate due to the contact pressure exerted by the sensor, the wave field caused by a point source at the origin of a cylindrical coordinate system is considered first. In this case, the distributed force is

$$q = [\delta(r)/2\pi r]f(t) \tag{30}$$

where $\delta(r)$ is the Dirac delta function, $f(t)$ is a time function, and $r = (x^2 + y^2)^{1/2}$.

Based on Eqs. (6) and (30) and using the Fourier–Hankel transform method (see Refs. 9 and 10), the frequency-domain solution of the wave field is

$$\bar{w} = -\frac{\bar{f}(\omega)}{4\pi D\delta_2^2}\left\{g_2(\omega)K_0\left(\sqrt{\delta_2^2 - \delta_1^2}r\right) + \frac{\pi}{2}g_1(\omega)\left[Y_0\left(\sqrt{\delta_1^2 + \delta_2^2}r\right) + iJ_0\left(\sqrt{\delta_1^2 + \delta_2^2}r\right)\right]\right\}, \qquad 0 < \omega < \omega_c \tag{31a}$$

$$\bar{w} = -\frac{\bar{f}(\omega)}{4\pi D\delta_2^2}\frac{\pi}{2}\left\{g_1(\omega)Y_0\left(\sqrt{\delta_1^2 + \delta_2^2}r\right) - g_2(\omega)Y_0\left(\sqrt{\delta_1^2 - \delta_2^2}r\right) + i\left[g_1(\omega)J_0\left(\sqrt{\delta_1^2 + \delta_2^2}r\right) - g_2(\omega)J_0\left(\sqrt{\delta_1^2 - \delta_2^2}r\right)\right]\right\} \qquad \omega > \omega_c \tag{31b}$$

in which

$$g_1(\omega) = 1 - (\omega/\omega_c)^2 + \left(c_p^2/\omega_C^2\right)\left(\delta_1^2 + \delta_2^2\right) \tag{32a}$$

$$g_2(\omega) = 1 - (\omega/\omega_c)^2 + \left(c_p^2/\omega_c^2\right)\left(\delta_1^2 - \delta_2^2\right) \tag{32b}$$

$$\delta_1^2 = \tfrac{1}{2}\left(1/c_p^2 + 1/k^2c_s^2\right)\omega^2 \tag{32c}$$

$$\delta_2^2 = \left[\tfrac{1}{4}\left(1/c_p^2 - 1/k^2c_s^2\right)\omega^4 + \left(1/\alpha^2c_p^2\right)\omega^2\right]^{\frac{1}{2}} \tag{32d}$$

$$c_p = \sqrt{E/\rho(1-\nu^2)} \tag{32e}$$

$$c_s = \sqrt{G/\rho} \tag{32f}$$

$$\omega_c = \sqrt{12k^2G/\rho h^2} \tag{32g}$$

$$\alpha^2 = h^2/12 \tag{32h}$$

where $J_0(x)$ and $Y_0(x)$ are the Bessel functions of order zero of the first and second kind and $K_0(x)$ is the modified Bessel function of the second kind of order zero.[11]

With the fundamental solution given, the frequency-domain solution of the scattered wave field in the plate due to the surface contact pressure exerted by the attached sensor can be obtained through integration over the sensor contact area.

When the general equations for the scattered [Eq. (9)] and incident [Eq. (8)] wave fields are considered and the superposition principle is used, the total wave field in the plate can be expressed as

$$w(x, y, t) = \bar{w}_s(x, y, \omega)e^{-i\omega t} + A_0\exp[i(\kappa_x x + \kappa_y y)]e^{-i\omega t} \tag{33}$$

To simplify the problem, the following assumptions according to Ref. 12 are introduced: 1) the pressure distribution exerted by the sensor can be approximated with a piston distribution and 2) the contact area between the transducer and the plate is so small that the transducer displacement corresponds to the plate deflection at the center of the contact area.

According to Fig. 2, the preceding assumptions and the traction-free boundary condition at the upper surface of the sensor yield

$$T_{zz1} = 0 \qquad \text{for} \qquad z_1 = 0 \tag{34a}$$

$$T_{zz1} = -p(t) \tag{34b}$$

$$w_1 = w(0, 0, t) \qquad \text{for} \qquad z_1 = h_1 \tag{34c}$$

where $p(t)$ is the magnitude of the contact stress between the sensor and the plate.

In view of the harmonic character of the incident wave, the frequency-domain expressions for Eqs. (34a–34c) are

$$\bar{T}_{zz1} = 0 \qquad \text{for} \qquad z_1 = 0 \tag{35a}$$

$$\bar{T}_{zz1} = -\bar{p}(\omega) \qquad \text{for} \qquad z_1 = h_1 \tag{35b}$$

$$\bar{w}_1 = A_0 \exp[i(\kappa_x x + \kappa_y y)] + H_{wp}\bar{p}(\omega) \qquad \text{for} \qquad z_1 = h_1 \tag{35c}$$

In which

$$H_{wp} = -\frac{1}{2D\delta_2^2}\int_0^a \left\{ g_2(\omega)K_0\left(\sqrt{\delta_2^2}-\delta_1^2 r_0\right) + \frac{\pi}{2} g_1(\omega)\left[Y_0\left(\sqrt{\delta_1^2+\delta_2^2}r_0\right) + iJ_0\left(\sqrt{\delta_1^2+\delta_2^2}r_0\right)\right]\right\} r_0\,\mathrm{d}r_0 \qquad 0<\omega<\omega_c \tag{36a}$$

$$H_{wp} = -\frac{\pi}{4D\delta_2^2}\int_0^a \left\{ g_1(\omega)Y_0\left(\sqrt{\delta_1^2+\delta_2^2}r_0\right) - g_2(\omega)Y_0\left(\sqrt{\delta_1^2-\delta_2^2}r_0\right) + i\left[g_1(\omega)J_0\left(\sqrt{\delta_1^2+\delta_2^2}r_0\right) - g_2(\omega)J_0\left(\sqrt{\delta_1^2-\delta_2^2}r_0\right)\right]\right\} r_0\,\mathrm{d}r_0, \qquad \omega>\omega_c \tag{36b}$$

where a is the radius of sensor. H_{wp} is obtained by using the fundamental solution (31a) and (31b) and integrating all contributions of the uniformly distributed pressure $p(t)$ exerted by the sensor over the circular contact area. The subscript wp indicates that the pressure p causes the displacement w.

Solution of Frequency-Response Functions

Substituting Eqs. (23) and (28) into Eqs. (35a) and (35b) and Eq. (22) into Eq. (35c) results in the following three equations:

$$\left[ic_1\bar{c}_{33}\omega + \mu_1(e^{ic_1\omega h_1}-1)\right]A_1 + \left[-ic_1\bar{c}_{33}\omega + \mu_1(e^{-ic_1\omega h_1}-1)\right]B_1 = 0 \tag{37a}$$

$$\left[ic_1\bar{c}_{33}\omega e^{ic_1\omega h_1} + \mu_1(e^{ic_1\omega h_1}-1)\right]A_1 + \left[-ic_1\bar{c}_{33}\omega e^{-ic_1\omega h_1} + \mu_1(e^{-ic_1\omega h_1}-1)\right]B_1 = -\bar{p} \tag{37b}$$

$$e^{ic_1\omega h_1}A_1 + e^{-ic_1\omega h_1}B_1 = A_0\exp[i(\kappa_x x+\kappa_y y)] + H_{wp}\bar{p} \tag{37c}$$

Solving for the three unknowns yields

$$A_1 = -\frac{\theta_{12}}{\theta_{11}\theta_{22}-\theta_{12}\theta_{21}}A_0\exp[i(\kappa_x x+\kappa_y y)] \tag{38a}$$

$$B_1 = \frac{\theta_{11}}{\theta_{11}\theta_{22}-\theta_{12}\theta_{21}}A_0\exp[i(\kappa_x x+\kappa_y y)] \tag{38b}$$

$$\bar{p} = \frac{\theta_{31}\theta_{12}-\theta_{32}\theta_{11}}{\theta_{11}\theta_{12}-\theta_{12}\theta_{21}}A_0\exp[i(\kappa_x x+\kappa_y y)] \tag{38c}$$

in which

$$\theta_{11} = ic_1\bar{c}_{33}\omega + \mu_1(e^{ic_1\omega h_1}-1) \tag{39a}$$

$$\theta_{12} = -ic_1\bar{c}_{33}\omega + \mu_1(e^{-ic_1\omega h_1}-1) \tag{39b}$$

$$\theta_{21} = e^{ic_1\omega h_1} + H_{wp}\left[ic_1\bar{c}_{33}\omega e^{ic_1\omega h_1} + \mu_1(e^{ic_1\omega h_1}-1)\right] \tag{39c}$$

$$\theta_{22} = e^{-ic_1\omega h_1} + H_{wp}\left[-ic_1\bar{c}_{33}\omega e^{-ic_1\omega h_1} + \mu_1(e^{-ic_1\omega h_1}-1)\right] \tag{39d}$$

$$\theta_{31} = ic_1\bar{c}_{33}\omega e^{ic_1\omega h_1} + \mu_1(e^{ic_1\omega h_1}-1) \tag{39e}$$

$$\theta_{32} = -ic_1\bar{c}_{33}\omega e^{-ic_1\omega h_1} + \mu_1(e^{-ic_1\omega h_1}-1) \tag{39f}$$

When Eqs. (38a) and (38b) are substituted into Eq. (28), the unknown $\gamma_1(\omega)$ is obtained as

$$\gamma_1 = \frac{\theta_{12}(1-e^{ic_1\omega h_1}) + \theta_{11}(e^{-ic_1\omega h_1}-1)}{\theta_{11}\theta_{22}-\theta_{12}\theta_{21}}\mu_1 A_0\exp[i(\kappa_x x+\kappa_y y)] \tag{40}$$

With Eq. (40), the frequency-domain solution of the output of the sensor is obtained from Eq. (27) as

$$\bar{V} = H_{Vhin}A_0\exp[i(\kappa_x x+\kappa_y y)] \tag{41}$$

in which

$$H_{Vhin} = \frac{i\omega d_{33}A\mu_1}{\chi^2 Y}\frac{\theta_{12}(1-e^{ic_1\omega h_1}) + \theta_{11}(e^{-ic_1\omega h_1}-1)}{\theta_{11}\theta_{22}-\theta_{12}\theta_{21}} \tag{42}$$

where H_{Vhin} is the frequency-response function (FRF) of the output voltage V of the sensor to a harmonic incident wave with amplitude A_0 and circular frequency ω.

Additionally, with Eqs. (41) and (38c), the voltage-pressure transduction function of the piezoelectric sensor is

$$T_{Vp} \equiv \frac{\bar{V}}{\bar{p}} = \frac{i\omega d_{33}A\mu_1}{\chi^2 Y}\frac{\theta_{12}(1-e^{ic_1\omega h_1}) + \theta_{11}(e^{-ic_1\omega h_1}-1)}{\theta_{31}\theta_{12}-\theta_{32}\theta_{11}} \tag{43}$$

Note that this transduction function does not depend on the properties of the plate, whereas Eq. (42) shows that the sensor voltage FRF is not only dependent on the sensor's inherent features, but also on the admittance of the attached electrical circuit and the characteristics of the plate.

Resonance Frequencies

To better understand the sensing characteristics of the piezoelectric transducer, the free vibration resonance frequencies of the sensor and the resonance frequency of the pressure-voltage transduction of the bonded sensor are discussed in the following paragraphs.

If the upper and lower surfaces of the sensor are considered to be stress free, Eqs. (23) and (25) yield the eigenvalue equation $\sin(c_1 h_1\omega) = 0$, that is, the resonance frequencies of the free–free piezoelectric sensor are

$$\omega_0 = n(\pi/c_1 h_1), \qquad n = 1, 2, 3, \ldots \tag{44a}$$

or

$$f_0 = \omega_0/2\pi = n/2c_1 h_1, \qquad n = 1, 2, 3, \ldots \tag{44b}$$

With Eq. (43), the pressure-voltage transduction of the sensor when the impedance of the attached electrical circuit is very large or the admittance $Y \approx 0$ is

$$T_{Vp} = -\frac{\chi^2}{d_{33}}\frac{\sin(c_1 h_1\omega/2)}{\cos(c_1 h_1\omega/2)} \tag{45}$$

Therefore, the resonance frequencies are the roots of $\cos(c_1 h_1\omega/2) = 0$, that is,

$$\omega^* = (2n-1)(\pi/c_1 h_1), \qquad n = 1, 2, 3, \ldots \tag{46a}$$

or

$$f^* = \omega^*/2\pi = (2n-1)/2c_1 h_1, \qquad n = 1, 2, 3, \ldots \tag{46b}$$

When Eqs. (44a) and (44b) and Eqs. (46a) and (46b) are compared, it is observed that the free–free vibration resonance frequencies are not the same as the resonance frequencies of the pressure-voltage transduction of the sensor, except for the first resonance frequency $n = 1$. The relationship between the two can be expressed as

$$\omega^* = 2\omega_0 - \pi/c_1 h_1 \tag{47a}$$

or

$$f^* = 2f_0 - 1/2c_1 h_1 \tag{47b}$$

The existence of these two kinds of resonance frequencies and their relationship are important for understanding the sensing characteristics of the sensors at higher frequencies.

FRF of Sensor with Backing Materials

To improve the sensitivity of an adhesively attached piezoelectric sensor, one may put some backing material on the upper surface of the sensor. In this section, the influence of the modification on the FRF of sensors is investigated.

Consider a sensor with an isotropic backing material as shown in Fig. 3. It is obvious that apart from traction-free boundary condition at the upper surface, all equations for the sensor and the plate in the preceding section are still valid. Referring to the coordinate system for the backing material as introduced in Fig. 3, we have the following additional equations corresponding to the equation of motion, the constitutive relation, and the upper surface boundary condition of the backing material

$$\frac{\partial T_{zz2}}{\partial z_2} = \rho_2 \frac{\partial^2 w_2}{\partial t^2} \tag{48}$$

$$T_{zz2} = E_2 \frac{\partial w_2}{\partial t} \tag{49}$$

$$T_{zz2} = 0 \qquad \text{for} \qquad z_2 = 0 \tag{50}$$

where w_2 and T_{zz2} denote the displacement and stress components along the thickness direction of the backing material and ρ_2 and E_2 are the mass density and Young's modulus, respectively.

The earlier traction-free condition at the upper surface of the sensor (34b) is replaced by the following two displacement and stress continuity conditions:

$$w_1 = w_2 \qquad \text{for} \qquad z_1 = 0, \qquad z_2 = h_2 \tag{51a}$$

$$T_{zz1} = T_{zz2} \qquad \text{for} \qquad z_1 = 0, \qquad z_2 = h_2 \tag{51b}$$

With these additional and modified equations and the application of a similar analysis procedure, the new FRF of the sensor with a backing material to a harmonic incident wave is obtained as

$$H_{Vhin} = \frac{i\omega d_{33} A \mu_1}{\chi^2 Y} \frac{\theta'_{12}(1 - e^{ic_1\omega h_1}) + \theta'_{11}(e^{-ic_1\omega h_1} - 1)}{\theta'_{11}\theta_{22} - \theta'_{12}\theta_{21}} \tag{52}$$

in which

$$\theta'_{12} = \theta_{11} + c_2 E_2 \omega \tan(c_2 h_2 \omega) \tag{53a}$$

$$\theta'_{12} = \theta_{12} + c_2 E_2 \omega \tan(c_2 h_2 \omega) \tag{53b}$$

It turns out that all of the solutions for the case of a sensor without backing materials can be applied, provided θ_{11} and θ_{12} as given in Eqs. (39a) and (39b) are replaced by the expressions just given. Thus, the pressure-voltage transduction function of a sensor with backing material can be written as

$$T_{Vp} \equiv \frac{\bar{V}}{\bar{p}} = \frac{i\omega d_{33} A \mu_1}{\chi^2 Y} \frac{\theta'_{12}(1 - e^{ic_1\omega h_1}) + \theta'_{11}(e^{-ic_1\omega h_1} - 1)}{\theta_{31}\theta'_{12} - \theta_{32}\theta'_{11}} \tag{54}$$

Numerical Results and Discussion

In this section, the simulation results of the sensing characteristics of adhesively bonded piezoelectric sensors attached to an isotropic plate are presented. If not otherwise stated, the material parameters of the plate are $\rho = 2700\ \text{kg/m}^3$, $E = 71.7 \times 10^9\ \text{N/m}^2$ and $\nu = 0.33$; the piezoelectric material characteristics are $s_{33}^E = 18.5 \times 10^{-12}\ \text{m}^2/\text{N}$, $d_{33} = 374 \times 10^{-12}\ \text{m/V}$, $\varepsilon_{33}^T = 15{,}045 \times 10^{-12}\ \text{F/m}$, and $\rho_1 = 7700\ \text{kg/m}^3$; and the backing material is copper with $\rho_2 = 8900\ \text{kg/m}^3$ and $E_2 = 117.2 \times 10^9\ \text{N/m}^2$.

In Fig. 4a, the influence of the thickness of the sensor is examined. Three sensors of different thickness ($h_1 = 5$, 3, and 2 mm) are considered. According to Eq. (44b), the first resonance frequencies of the free vibration for these three sensors are calculated to be $f_0 =$ 0.376, 0.626, and 0.94 MHz, and, according to Eq. (32g), the cutoff frequency of the 2-mm-thick plate is 0.807 MHz. Figure 4a shows that the frequencies corresponding to the three peaks are 0.36, 0.58, and 1.05 MHz, which do not correspond to any of the preceding special frequencies. This clearly demonstrates that the knowledge

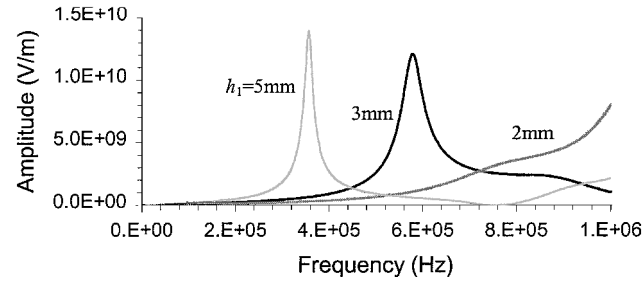

Fig. 4a Voltage FRF H_{Vin} of sensors with different thickness: plate thickness $h = 2$ mm, sensor diameter $a = 3$ mm, and electrical admittance of measurement circuit $Y = 10^{-7}$ 1/Ω.

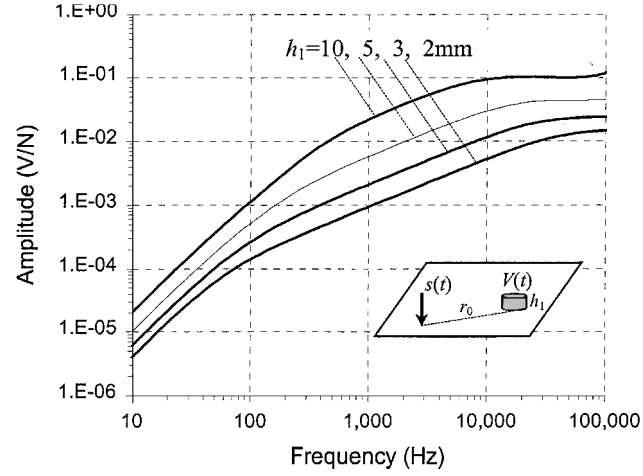

Fig. 4b Low-frequency regime of voltage FRF $H_{Vin} = \bar{V}/\bar{s}$ of sensors with different thickness for normal point force input: source–sensor distance $r_0 = 0.2$ m, plate thickness $h = 2$ mm, sensor diameter $a = 3$ mm, and electrical admittance of measurement circuit $Y = 10^{-7}$ 1/Ω.

of the sensor's free vibration behavior is not sufficient to predict accurately its frequency response characteristics when it is attached to a structure. Additionally, it is seen that, as expected, thicker sensors are more sensitive in the low-frequency region and that their first resonance frequency is narrowband compared to thinner sensors.

In Fig. 4b, the results of the voltage FRF for sensors with different thickness are shown for frequencies below 100 kHz. In this simulation the flexural waves are generated by a normal point force $s(t)$, which is located a distance $r_0 = 0.2$ m away from the sensor. The normal point force $s(t)$ can be an arbitrary function in time, and the voltage FRF H_{Vin} is defined as the ratio of the voltage output frequency spectrum $\bar{V}$ to the normal point force input frequency spectrum $\bar{s}$. This modification has no influence on the character of the results compared to the case with a general harmonic wave input, which is used in all other simulations. However, it represents a typical experimental configuration used to determine the FRF of piezoelectric sensors and, therefore, is better suited to be compared with experimental data, which may be found in the literature. The results show that, even in the low-frequency regime, the thickness of the sensor has a significant influence on the sensitivity of the measurement system. This emphasizes the relevance of the piezodynamic model because a conventional rigid sensor model[13] would not be able to predict these results. Therefore, the quantitative analysis of experimental results or the optimization of a specific measurement configuration would not be possible.

In Fig. 5, the influence of the flexural stiffness of the structure is examined. It is observed that a thicker substrate results in a larger response amplitude but shows a narrow resonance peak compared to a thinner plate. This shows again that the complex sensor–substrate interaction processes dominate the overall behavior of the measurement system and that the detailed knowledge of them is essential to enable the quantitative prediction of experimental observations and the optimization of the measurement system.

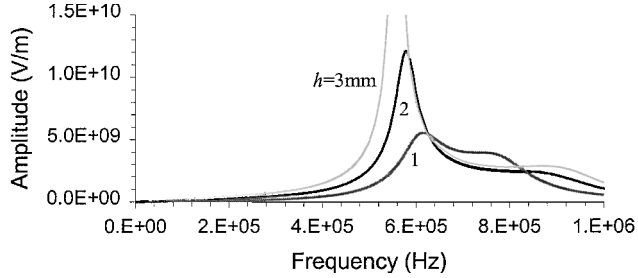

Fig. 5 Voltage FRF H_{Vin} of sensor attached to plates with different thickness: sensor thickness h_1 = 2 mm, sensor diameter a = 3 mm, and electrical admittance of measurement circuit $Y = 10^{-7}$ 1/Ω.

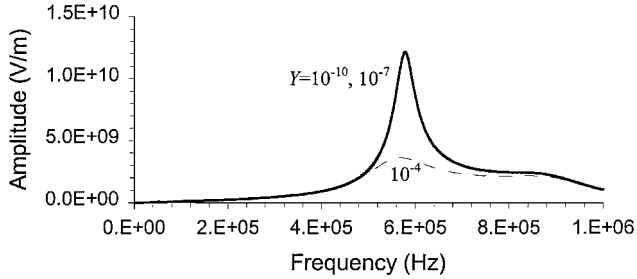

Fig. 6 Voltage FRF H_{Vin} of sensors attached to electrical circuits with different admittance: plate thickness h = 2 mm, sensor thickness h_1 = 2 mm, and sensor diameter a = 3 mm.

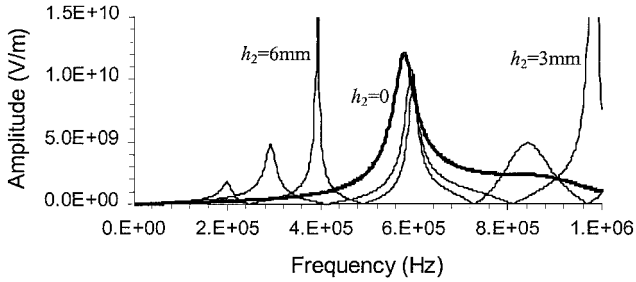

Fig. 7 Voltage FRF H_{Vin} of sensors with copper backings of different thickness: plate thickness h = 2 mm, sensor thickness h_1 = 2 mm, sensor diameter a = 3 mm, and electrical admittance of measurement circuit $Y = 10^{-7}$ 1/Ω.

Figure 6 shows the influence of the admittance of the attached electrical circuit on the measurement system's performance. It turns out that its influence is restricted to a small frequency range around the resonance frequency. Note, however, that it may have a pronounced influence on the system's sensitivity if the admittance becomes large, that is, if the sensor is coupled to an electrical circuit with low impedance.

In Fig. 7, the influence of copper backing on the sensor's voltage output is examined. As expected, the backing material has a significant influence on its sensitivity and frequency response. More resonance frequencies exist within a given frequency regime, and the first resonances are shifted to lower frequencies. Therefore, by carefully choosing the backing material for a sensor attached to a specific structure, it is possible to optimize the performance of the measurement system.

To simplify the analysis of a sensor's sensitivity to incoming flexural waves, the sensor has been modeled as a rigid disk before.[13] For the purposes of checking the validity of this simplified analysis method, the pressure sensed by a sensor is evaluated both by the rigid mass model and by the present elastic continuum model. The comparison of the two results for the case of a sensor with and without backing material are given in Figs. 8a and 8b, respectively. The results show that the two models are in good agreement away from the system's resonance frequencies. However, because the rigid sensor model is not able to represent the wave reflections within the sensor,

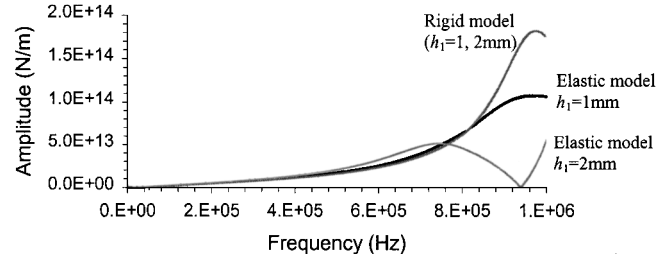

Fig. 8a FRF of normalized contact pressure $\bar{p}/\bar{A}_0$ of two sensors of different thickness, calculated by present elastic continuum model and simplified rigid sensor model: plate thickness h = 2 mm, sensor diameter a = 3 mm, and electrical admittance of measurement circuit $Y = 10^{-7}$ 1/Ω (without copper backing).

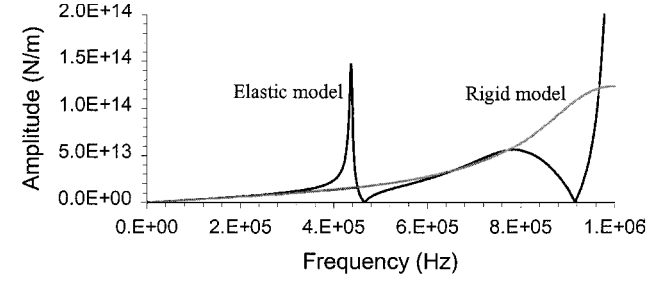

Fig. 8b FRF of normalized contact pressure $\bar{p}/\bar{A}_0$ of sensor, calculated by present elastic continuum model and simplified rigid sensor model: plate thickness h = 2 mm, sensor thickness h_1 = 1 mm, sensor diameter a = 3 mm, and electrical admittance of measurement circuit $Y = 10^{-7}$ 1/Ω (with copper backing, h_2 = 3 mm).

it is no longer valid around the resonance frequencies and should, therefore, be avoided when predicting the sensor's characteristics, especially for thicker sensors and sensors with backing materials.

Conclusions

The wave sensing problem for contact-type sensors used in the traveling wave control techniques has been investigated. With the dynamic theory of piezoelectricity, Mindlin plate wave motion theory, and a multiple integral transform method, the voltage output FRF of piezoelectric sensors, with and without backing materials, adhesively attached to a plate, to incoming flexural waves has been developed. The results of the numerical simulations have shown the following:

1) The sensitivity of a piezoelectric sensor attached to a structure not only depends on the properties of the sensor itself, but also on the characteristics of the tested structure and the admittance of the attached electric circuit. Hence, for maximum sensitivity of the traveling wave control technique, it is required that the sensors be designed according to the characteristics of the structure to be controlled, the electric characteristics of the attached measurement device, and the frequency range of the external disturbance.

2) Adding a backing material to a piezoelectric sensing element changes its frequency-response characteristics, especially in the low-frequency regime. This may provide some additional flexibility to optimize the sensitivity of the measurement system. However, it also makes its behavior more complicated because more resonance frequencies occur. Thus, backing materials need to be chosen properly, by quantitative analysis, to achieve maximum sensitivity in the frequency regime of interest.

3) Provided that the admittance of the attached electric circuit is very small (i.e., its impedance is very large), its influence on the sensitivity of the sensor can be neglected.

4) The simplified rigid mass model for a sensor can be used to characterize the sensitivity of the measurement system away from its resonance frequencies. However, it is no longer valid around the resonance frequencies and should, therefore, be avoided when predicting the sensor's characteristics, especially for thicker sensors and sensors with backing materials.

Acknowledgment

This work has been supported by the Australian Research Council under Grant A89937136.

References

[1]Fuller, C. R., Elliott, S. J., and Nelson, P. A., *Active Control of Vibration*, Academic Press, New York, 1996, pp. 25–302.

[2]Miller, D. W., and Hall, S. R., "Experimental Results Using Active Control of Traveling Wave Power Flow," *Journal of Guidance, Control, and Dynamics*, Vol. 14, No. 2, 1991, pp. 350–359.

[3]Pan, X., and Hansen, C. H., "The Effect of Error Sensor Location and Type on the Active Control of Beam Vibration," *Journal of Sound and Vibration*, Vol. 165, No. 3, 1993, pp. 497–510.

[4]Fujii, H. A., Nakajima, K., and Matsuda, K., "Wave Approach for Control of Orientation and Vibration of a Flexural Structure," *Journal of Guidance, Control, and Dynamics*, Vol. 19, No. 3, 1996, pp. 578–583.

[5]Prakah-Asante, K. O., and Craig, K. C., "Active Control Wave-Type Vibration Energy for Improved Structural Reliability," *Applied Acoustics*, Vol. 46, No. 1, 1995, pp. 175–195.

[6]Tiersten, H. F., *Linear Piezoelectric Plate Vibrations*, Plenum, New York, 1969, pp. 33, 34.

[7]Ristic, V. M., *Principles of Acoustic Devices*, Wiley, New York, 1983.

[8]Miklowitz, J., "Flexural Stress Waves in an Infinite Elastic Plate Due to a Suddenly Applied Concentrated Transverse Load," *Journal of Applied Mechanics*, Vol. 27, No. 4, 1960, pp. 681–689.

[9]Sneddon, I. N., *Fourier Transforms*, McGraw–Hill, New York, 1951, pp. 1–9.

[10]Miklowitz, J., *The Theory of Elastic Waves and Waveguides*, North-Holland, Amsterdam, 1978, pp. 231–290.

[11]Gradshteyn, I. S., and Ryzhik, I. M., *Table of Integrals, Series, and Products*, Academic Press, New York, 1980, pp. 960, 961.

[12]Williams, J. H., Karagulle, J. H., and Lee, S. S., "Ultrasonic Input–Output for Transmitting and Receiving Longitudinal Transducers Coupled to Same Face of Isotropic Elastic Plate," *Materials Evaluation*, Vol. 40, No. 6, 1982, pp. 655–662.

[13]Liu, T., Liew, K. M., and Kitipornchai, S., "Analysis of Acousto-Ultrasonic Characteristics for an Isotropic Thin Plate," *Journal of the Acoustical Society of America*, Vol. 105, No. 6, 1999, pp. 3318–3325.